Title: Magnetic nanoparticles in MCM-41 type mesoporous silica

Author: Marian Surowiec, Bożena Bierska-Piech, M. Wiertel, M. Budzyński, J. Goworek

Citation style: Surowiec Marian, Bierska-Piech Bożena, Wiertel M., Budzyński M., Goworek J. (2008). Magnetic nanoparticles in MCM-41 type mesoporous silica. "Acta Physica Polonica A" (Vol. 114, nr 6 (2008), s. 1605-1613).

Proceedings of the Polish Mössbauer Community Meeting 2008

Magnetic Nanoparticles in MCM-41 Type Mesoporous Silica

Z. Surowiec[a], B. Bierska-Piech[b], M. Wiertel[a], M. Budzyński[a] and J. Goworek[c]

[a]Institute of Physics, M. Curie-Skłodowska University
pl. M. Curie-Skłodowskiej 1, 20-031 Lublin, Poland
[b]Institute of Materials Science, University of Silesia
Bankowa 12, 40-007 Katowice, Poland
[c]Department of Adsorption, Faculty of Chemistry
Maria Curie-Skłodowska University
pl. M. Curie-Skłodowskiej 1, 20-031 Lublin, Poland

Structural phase transformations and magnetic properties of mesoporous MCM-41 template modified with iron and nickel salts were studied by nitrogen physisorption, X-ray diffraction, Mössbauer spectroscopy and transmission electron microscopy. The FeNi-oxide or the bimetallic crystal structure is formed for low and high Ni concentrations, respectively. The average size of nanoparticles is about 10 nm. About 70% of particles exist in a superparamagnetic state at room temperature.

PACS numbers: 78.67.Bf, 81.07.Bc, 76.80.+y

1. Introduction

In the last decade iron-modified mesoporous MCM-41 silica materials have received significant attention as new nanostructured and catalyst materials [1–3]. Different methods for their preparation by direct synthesis [4] or post-synthesis modification [5, 6] have been described. Mesoporous materials can be used conveniently as templates to obtain magnetic compounds in low-dimensional arrays.

In metal nanoparticles, size is the only control to their superparamagnetic properties, and the superparamagnetic state is usually observed in metal particles within a few nanometer size ranges. The applications of the superparamagnetic metal nanoparticles also are limited due to the chemical instability of pure metals. Superparamagnetic properties of materials are determined by magnetic anisotropy, which comes from electron spin–orbital angular momentum coupling at lattice sites in the crystal structure. The dominant factors that control the strength of magnetic couplings are the magnitude of magnetic moment on each coupling component, the distance between them, and the symmetry of the lattice site. These

factors correspond to the crystal structure issues of chemical composition, lattice constant, and coordination environment at the lattice sites. In pure metal this crystal chemistry are fixed. The crystal chemistry can be varied in a controlled fashion in metal oxides. Spinel ferrite, MFe_2O_4 (M = Fe, Ni, Cu or Mg) is a particularly important magnetic material system.

This paper presents the results of MCM-41 template impregnation with Fe and Ni carrying organic salts in appropriate ratios. Structural and magnetic properties were investigated particularly taking the finite-size effects into account.

2. Experimental

2.1. Synthesis of materials

The synthesis of organo-silica-materials with incorporated alkyl chains silicas was accomplished using the procedure described in [7] with the use of octadecyltrimethylammonium bromide (Aldrich) as a structure directing agent (surfactant). As a silica source tetraethoxysilane (TEOS) (Aldrich) was used. The surfactant forming the template was dissolved in deionized water to give a 0.055 mol dm^{-3} solution and 9.5 g of aqueous ammonia (POCh, Poland) were added into the solution while stirring. TEOS was added dropwise to this solution and stirred at 323 K for 1 h. The resultant solid products were filtered and washed with hot distilled water and dried in air at 363 K for 24 h. Template removal from MCM-41 was carried out by extraction at 363 K.

About 1 g of as-synthesized material was combined with 50 cm^3 of propanol and refluxed in soxhlet for 12 h. Then the product was isolated by filtration and dried at 333 K for 24 h. The as-synthesized material was placed in a porcelain crucible and calcinated in air at 823 K for 8 h.

The next step of preparation was impregnation. 5% aqueous solutions were prepared from the salts: $Fe(NO_3)_3 \cdot 9H_2O$ and $Ni(NO_3)_2 \cdot 6H_2O$. In order to prepare a bimetallic system on the support MCM-41, 5% solution containing metal ions (Fe^{3+} and Ni^{2+}) was mixed in proper ratios and the samples were prepared by means of co-impregnation. Then the samples were subjected to low temperature treatment (drying) at 150°C for 1 h. The next stage was calcination in air atmosphere 300°C for 1 h. As a result of such a procedure there should be formed oxide systems deposited on MCM-41 of the general formula Fe_3O_4–NiO/MCM-41. The investigated samples were as Fe–Ni_x/MCM-41where x is the assumed contribution of %Ni in relation to Fe. The last stage of high temperature treatment was reduction in hydrogen atmosphere at 300°C for 4 h. The heating and cooling time was 40 min.

2.2. Methods and apparatus

The samples were investigated by transmission electron microscopy (TEM) using a JEOL JEM 3010 microscope operated at 300 kV. The powder was ground in alcohol and spread over a carbon grid.

The X-ray difraction (XRD) patterns were studied by the Philips X'Pert PW 3040/60 X-ray diffractometer with Cu K_α radiation.

The ^{57}Fe Mössbauer spectra of the investigated samples were measured at room temperature (RT) using a constant acceleration spectrometer in a transmission mode with the ^{57}Co/Rh source. The isomer shift, δ, was calibrated against a metallic iron foil at room temperature.

3. Results and discussion

Nitrogen adsorption measurements were carried out for the MCM-41 template. Specific surface area (S), average pore diameter (R) and specific pore volume (V) were determined. The values of the above mentioned physical quantities are equal to: $S = 1214$ m^2/g, $R = 1.5$ nm and $V = 0.93$ cm^3/g, respectively [7].

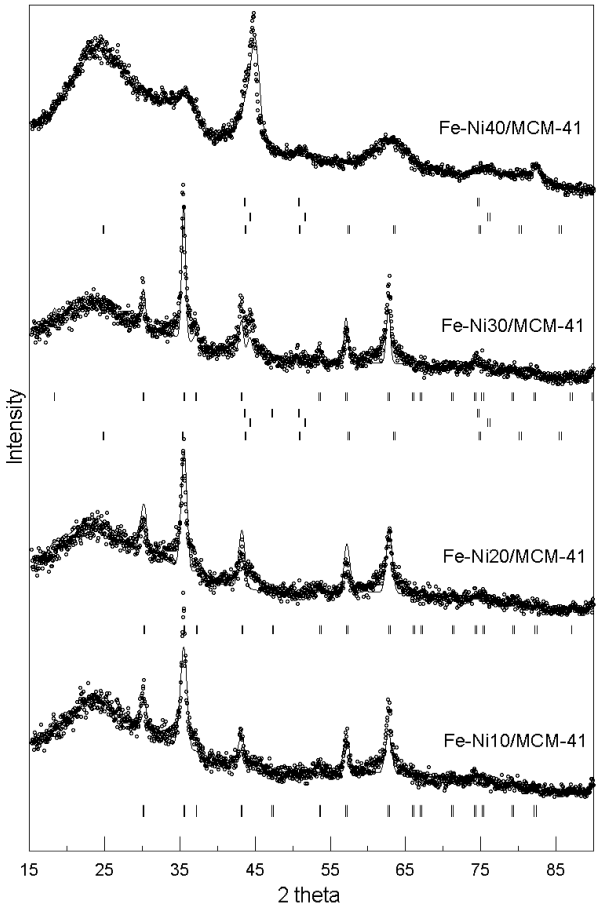

Fig. 1. The XRD diffraction pattern of crystalline in the MCM-41 silicate template. The full curve represents calculated pattern, the points the observed one. Short vertical lines below the diffraction pattern indicate the calculated Bragg positions.

The XRD measurements were carried out in order to obtain information about changes in the structures of crystallites embedded in the mesoporous silica template. The X-ray diffraction patterns of all samples are shown in Fig. 1. The smoothly varying peak intensity in the 10°–30° range results from the amorphous silica template. The sharp peaks correspond to the diffraction on the nanocrystallites. The XRD patterns of Fe–Ni_{10}/MCM-41 and Fe–Ni_{20}/MCM-41 materials

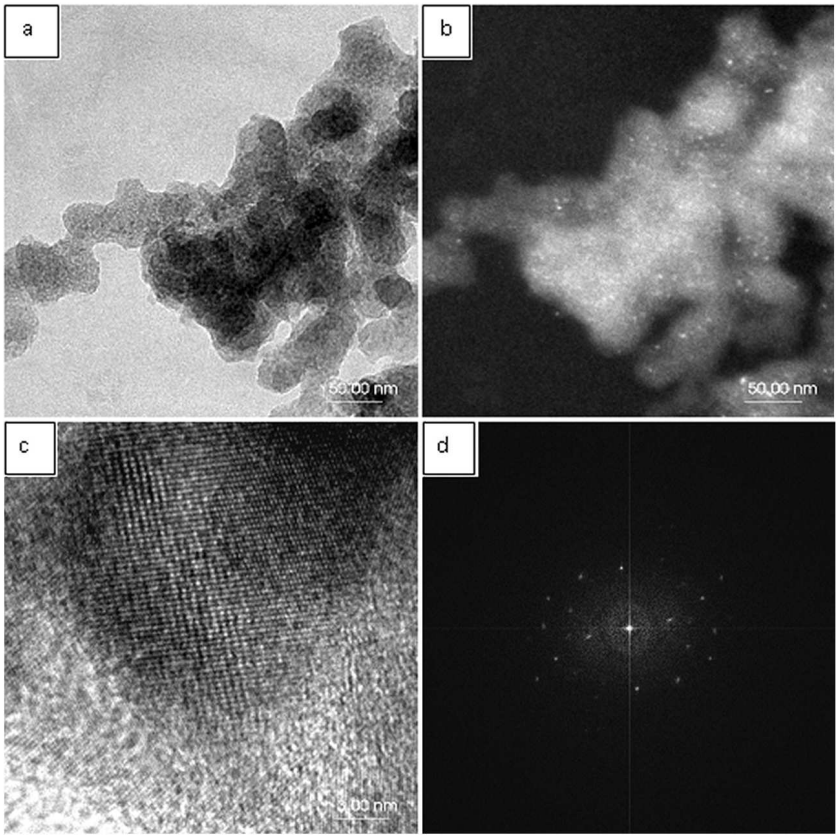

Fig. 2. Transmission electron microscope images: general view (a), high resolution image of an ordered MCM-41 grain with the electron diffraction pattern (b), and Fe–Ni_{10}/MCM-41 particle (c) with the electron diffraction pattern (d).

TABLE I

Crystal structure parameters of Fe–Ni_{40}/MCM-41 samples.

Index name	Empirical formula	Crystal system	Space group	Lattice constant
iron nickel	$Fe_{0.94}Ni_{0.06}$	cubic	$Im3m$	2.868 [Å]
iron nickel	$Fe_{0.64}Ni_{0.36}$	cubic	$Fm3m$	3.592 [Å]
iron nickel	$Fe_{0.55}Ni_{0.44}$	cubic	$Pm3m$	3.590 [Å]

show some typical *hkl* reflections of the magnetite-like structure. The lattice parameters are 8.37(1) Å and 8.38(1) Å, respectively. These parameters are very similar to that in the bulk magnetite ($a = 8.39(1)$ Å) but somewhat larger than for Fe_3O_4/MCM-41 ($a = 8.34(1)$ Å) [8]. The increase in Ni content up to 30% in relation to Fe causes an additional crystal phases formation. These crystal phases were identified as the bimetallic Fe–Ni structures. However, in the Fe–Ni_{40}/MCM-41 sample, the diffraction lines characteristic of oxide with the spinel structure were not observed. From the analysis of Fe–Ni_{40}/MCM-41 XRD pattern, three different Fe–Ni bimetallic phases were identified (see Table I). Particularly large broadening of the XRD diffraction lines in this sample indicates the occurrence of crystallites of very small sizes.

Figure 2a shows the representative TEM images obtained for the Fe–Ni_{10}/MCM-41 sample. Rounded grains of disordered MCM-41 support of the sizes from 30 to 50 nm are seen. Figure 2c obtained with the sixteenfold higher magnification, demonstrates a picture of a single nanocrystal. Electron diffraction patterns corresponding to these figures are presented in Figs. 2b and d. They reveal the fourfold symmetry of nanocrystallites specific to a cubic crystal structure. From the TEM data the average size of crystallite grains was determined as equal approximately to 10 nm.

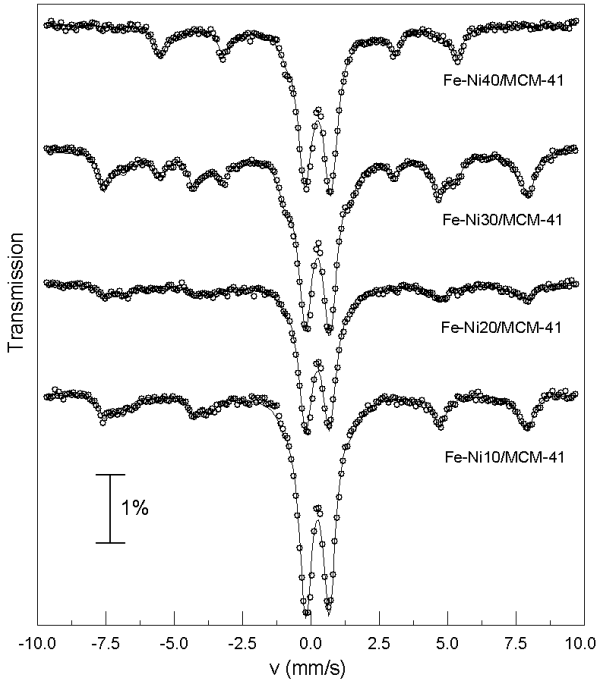

Fig. 3. The ^{57}Fe Mössbauer spectra for the samples located in the MCM-41 silicate template at room temperature.

TABLE II

The Mössbauer parameters of Fe–Ni_x/MCM-41 samples. Sxt. — sextet, dbl. — doublet.

Sample	Crystal structure	Component	IS [mm/s]	QS [mm/s]	H [T]	G [%]
Fe–Ni_{10}/ MCM-41	spinel	sxt. Fe^{3+}(tet.)	+0.29	–0.015	48.4	12
		sxt. Fe^{2+}(oct.)	+0.57	0.12	45.4	16
		dbl.	+0.33	0.86		72
Fe–Ni_{20}/ MCM-41	spinel	sxt. Fe^{3+}(tet.)	+0.31	0.02	48.3	9
		sxt. Fe^{2+}(oct.)	+0.58	0.19	44.8	13
			+0.32	0.86		78
Fe–Ni_{30}/ MCM-41	spinel	sxt. Fe^{3+}(tet.)	+0.29	–0.00	48.4	16
		sxt. Fe^{2+}(oct.)	+0.52	0.017	45.2	13
	inter-metallic	sxt.	0.00	0.07	33.7	15
	inter-metallic	sxt.	0.02	0.02	27.0	6
		dbl.	+0.33	0.89		50
Fe–Ni_{40}/ MCM-41	inter-metallic	sxt.	+0.02	– 0.083	33.9	12
	inter-metallic	sxt.	– 0.02	0.022	30.3	19
		dbl.	+0.33	0.93		68

The Mössbauer spectra of the iron–nickel nanocrystals formed in the MCM-41 type silicate templates at room temperatures are shown in Fig. 3. Corresponding hyperfine parameters for different components of the Mössbauer spectra are presented in Table II. The experimentally obtained patterns consist of sextets and a superimposed doublet. In the Fe–Ni_{10}/MCM-41 and Fe–Ni_{20}/MCM-41 materials the parameters of the sextet components are close to those of Fe_3O_4. The sextets originate from Fe atoms located at two non-equivalent tetrahedral (A) and octahedral (B) sites in the magnetite-like structure. The Fe^{2+}/Fe^{3+} ratio was determined by using the relative areas of the elementary patterns representing the microenvironments of Fe^{2+} and Fe^{3+}. The occupation ratio of the cations in A and B sites is distinct for different Ni contents in the sample. In the Fe–Ni_{10}/MCM-41 and Fe–Ni_{20}/MCM-41 materials the occupation ratio is about 2:1 and 1:1, respectively. However, in the bulk the ratio is 1:2. The similar effect was observed in the nanowire arrays at anodizing anodic alumina oxide [9].

The doublet component is related to the superparamagnetic phase of the iron oxide. The existence of the superparamagnetic nanoparticles results from the relaxation phenomenon due to the intrinsic finite-size effect. The line broadening

of the sextets is typical of superparamagnetic nanoparticles close to the blocking temperature which is defined as the transition temperature from fast to slow relaxation [10, 11]. The relaxing component contributes to the relative area of about $75 \pm 5\%$ to the total spectrum at room temperature.

The Mössbauer spectrum for the Fe–Ni_{30}/MCM-41 system reflects the mixed spinel and bimetallic structure observed in the XRD pattern. However, the spectrum of Fe–Ni_{40}/MCM-41 materials consists of the absorption lines originating from Fe–Ni crystallites.

In Fig. 4 the Mössbauer spectra of the Fe–Ni_{40}/MCM-41 sample at different temperatures are presented. With the increasing temperature the ferrimagnetic

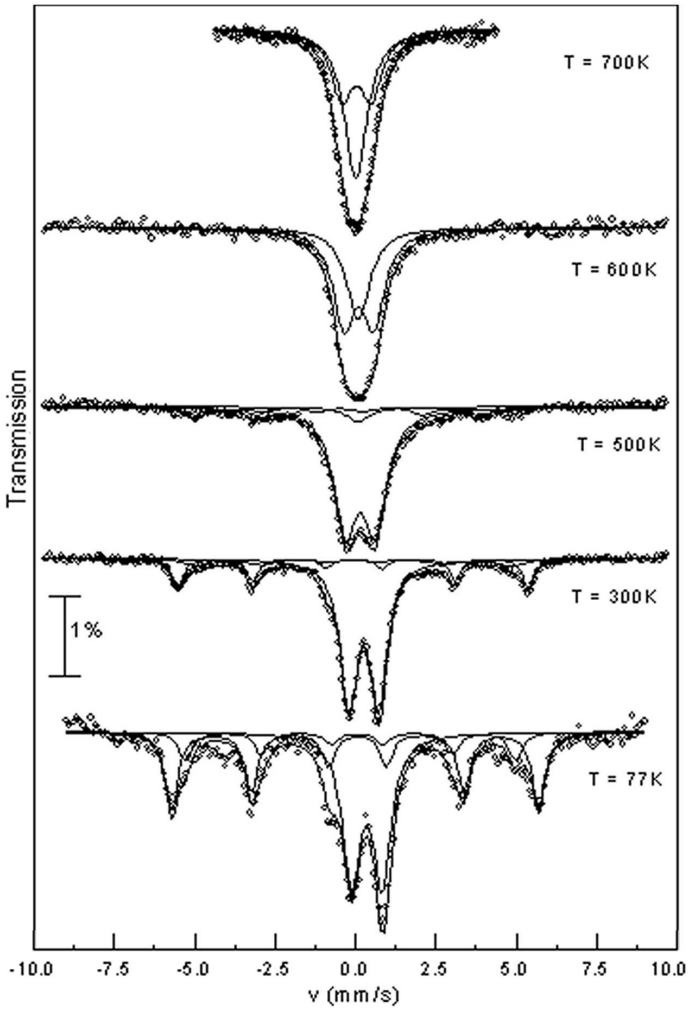

Fig. 4. The ^{57}Fe Mössbauer spectra for the Fe–Ni_{10}/MCM-41 sample at some selected temperatures.

component decreases. Additionally, a monoline appears in the Mössbauer spectra recorded at the temperatures above 500 K. This phenomenon can be explained by the core-shell model [12]. The doublet with a significant quadrupole splitting value equal to 0.93(3) mm/s originates from ^{57}Fe nuclear probes in the non-spherical local surroundings occurring in the surface shells of the particles. The higher distortion of the iron polyhedra at the surface layer could be due to the ions possessing a higher degree of ligand coordination distortion and to their interactions with the support. The monoline results from nanoparticles in the superparamagnetic state in a similar way to the doublet. However, in this case ^{57}Fe probes located in the core of nanoparticles are a source of signal. They have spherical local surroundings in which there is no electric field gradient.

4. Conclusions

As follows from the investigations the method of the Fe–Ni nanocrystallites preparation by MCM-41 template impregnation in a suitable solution in the concentrations range of $x \leq 0.30$, nanocrystallites of spinel structure are obtained. For $x = 0.40$ the nanostructure material consists of bimetallic Fe–Ni particles with three different cubic structures. The XRD and Mössbauer results allow concluding that both iron–nickel species occur in two magnetic states. A high percentage of smaller particles exists in the superparamagnetic state and a remaining part of larger particles is in the ferromagnetic state. An increase in superparamagnetic phase contribution relative to the magnetic one with the increase in temperature is caused by a larger and larger number of relaxing magnetic particles. Occurrence of the doublet and monoline in the Mössbauer spectra can be explained by the core-shell model below the Curie temperature.

Acknowledgments

The authors thank Dr. K.M. Prusik for the transmission electron microscopy measurements.

References

[1] M.V. Cagnoli, A.M. Alvarez, J.F. Bengoa, N.G. Gallegos, L.V. Mogni, M.X. Gonzalez Oddera, S.G. Marchetti, R.C. Mercader, *Hyperfine Interact.* **148/149**, 185 (2003).

[2] J.F. Bengoa, M.V. Cagnoli, N.G. Gallegos, A.M. Alvarez, L.V. Mogni, M.S. Moreno, S.G. Marchetti, *Mikropor. Mesopor. Mater.* **84**, 153 (2005).

[3] R. Kohn, M. Froba, *Catal. Today* **68**, 114 (2001).

[4] M. Stockenhuber, R.W. Joyner, J.M. Dixon, M.J. Hudson, G. Grubert, *Mikropor. Mesopor. Mater.* **44/45**, 367 (2001).

[5] P. Selvam, S.E. Dapurkar, S.K. Badamali, M. Murugasan, H. Kuwano, *Catal. Today* **68**, 69 (2001).

[6] N.A. Fellenz, J.F. Bengoa, S.G. Marchetti, F.R. Sives, S.J. Stewart, R.C. Mercater, *Hyperfine Interact.* **170**, 75 (2006).

[7] J. Goworek, W. Stefaniak, A. Kierys, M. Iwan, *J. Therm. Anal. Cal.* **87**, 217 (2007).

[8] Z. Surowiec, J. Goworek, J. Ryczkowski, M. Budzyński, M. Wiertel, J. Sarzyński, *Nukleonika* **52**, S33 (2007).

[9] D.S. Xue, F.S. Li, *Hyperfine Interact.* **156/157**, 31 (2004).

[10] K.A. Malini, M.R. Anantharaman, A. Gupta, *Bull. Mater. Sci.* **27**, 361 (2004).

[11] S.M. Kamali, T. Ericsson, R. Wäpling, *Thin Solid Films* **515**, 721 (2006).

[12] A.M. Van der Kraan, *Hyperfine Interact.* **40**, 211 (1988).